SiC/MCM-48 and SiC/SBA-15 Nanocomposite Materials

Piotr Krawiec,† Claudia Weidenthaler, and Stefan Kaskel*,†

Max-Planck-Institut für Kohlenforschung, Kaiser-Wilhelm-Platz 1, D 45470 Mülheim an der Ruhr, Germany

Received August 8, 2003. Revised Manuscript Received December 5, 2003

Silicon carbide (SiC) was infiltrated into the ordered mesoporous molecular sieves MCM-48 and SBA-15 using chemical vapor infiltration (CVI) of dimethyldichlorosilane (DDS) and hydrogen as the carrier gas. The infiltration process was followed ex situ using nitrogen physisorption measurements, small- and wide-angle X-ray diffraction, X-ray photoelectron spectroscopy, IR spectroscopy, and transmission electron microscopy. For MCM-48, infiltration at lower temperatures (1023 K) affords a thin, X-ray amorphous, SiC-based coating on the inner surface of the molecular sieve and the pore size of the mesoporous host decreases from 2.4 nm into the micropore regime (<2 nm). At higher temperature (1163 K), the deposition of 20−30-nm sized β-SiC particles is observed on the outer surface of the mesoporous particles as a process competitive to the pore filling. The crystalline nanoparticles form a hard protective coating on the outer surface of the larger spherical MCM-48 particles resembling hedgehog-like core−shell particles composed of an inner ordered mesoporous matrix and a hard nanosized silicon carbide coating. For SBA-15 it is shown that in the early stages of the CVI process at 1118 K, an ultrathin coating is produced that mainly consists of silicon oxycarbide. Subsequently, X-ray amorphous SiC is formed on top of this coating. In SBA-15, along with the formation of the coating, the pore size decreases from 5.5 to 3.0 nm, but further deposition leads to inhomogeneous coatings, and pore blocking and crystalline β-SiC particles are detected on the outer surface of the porous matrix by means of dark field transmission electron microscopy and wide-angle X-ray diffraction. The CVI process results in a significant enhancement of the thermal stability of SBA-15 even for very small degrees of filling.

Introduction

Nanocomposites have received considerable attention in recent years.[1] The integration of a second component into a host matrix system allows for the combination of physical or chemical properties that cannot be achieved by modification of the matrix alone. Examples are the combination of hard and elastic materials for the fabrication of materials with good scratch resistance and flexibility, the incorporation of a fire retardant into plastics to reduce the flammability, or the coating of insulators with electron conducting materials for the manufacture of anti-static coatings. A crucial issue is to control the size and dimension of the second component or guest material, because optical as well as mechanical properties critically depend on the dimensions of the microstructure. One way to predefine the dimensions of the included material is to use porous matrixes as host materials that limit the extended growth of crystals and allow predetermination of the composite architecture by adjusting the pore size and arrangement of the pore system. In this respect, ordered mesoporous ($d = 2-50$ nm) host systems such as MCM-48 and SBA-15 are especially valuable, as their pore size can be controlled within a range of only a few nanometers. The pore system is periodic and three-dimensional long-range ordered, which guarantees not only a narrow pore size distribution, but also a well-defined composite architecture. Whereas cationic surfactants such as cetyltrimethylammonium bromide (CTAB) do not allow extension of the pore size beyond 40 Å without using swelling agents, large pore mesoporous silicas with hexagonal pore arrangements (SBA-15) were developed by Stucky using the triblock copolymers.[2] The pore size can be adjusted in a wide range between 40 and 300 Å. Large pores are beneficial for catalytic applications because they allow the processing of heavy residues and the encapsulation of biomolecules such as enzymes.

Nanoporous matrixes can be infiltrated using liquid or vapor-phase infiltration techniques. Liu has studied the infiltration of MCM-41 for the preparation of platinum nanowires.[3] After the infiltration and thermal decomposition of the precursor, the matrix was removed with HF. Chemical vapor infiltration of MCM-48 has been used for the manufacture of porous palladium superlattice nanoballs and nanowires[4] and Pd/MCM-48 nanocomposites.[5] MCM-41 was also used for a space-

* To whom correspondence should be addressed. E-mail: Stefan.Kaskel@chemie.tu-dresden.de. Phone: 49-351-46334885. Fax: 49-351-46337287.

† Current address: Institut für Anorganische Chemie Technische Universität Dresden, Mommsenstr. 6, 01069 Dresden, Germany.

(1) Zhang, S.; Sun, D.; Fu, Y. Q.; Du, H. J. *Surf. Coat. Technol.* **2003**, *167*, 113−119.

(2) Zhao, D. Y.; Huo, Q. S.; Feng, J. L.; Chmelka, B. F.; Stucky, G. D. *J. Am. Chem. Soc.* **1998**, *120*, 6024−6036.

(3) Liu, Z.; Sakamoto, Y.; Ohsuna, T.; Hiraga, K.; Terasaki, O.; Ko, C. H.; Shin, H. J.; Ryoo, R. *Angew. Chem., Int. Ed.* **2000**, *39*, 3107−3110.

(4) Kang, H.; Jun, Y.; Park, J. I.; Lee, K. B.; Cheon, J. *Chem. Mater.* **2000**, *12*, 3530−3532.

10.1021/cm034737+ CCC: $27.50 © 2004 American Chemical Society
Published on Web 06/29/2004

confined synthesis of GaN nanoparticles using liquid and gas-phase infiltration techniques.[6,7] Fröba has studied the formation of $Cd_{1-x}Mn_xS$ particles in MCM-41.[8] Crystalline ZrO_2 nanoparticles with well-defined particle size can be synthesized in SBA-15 matrixes.[9] Large-pore mesoporous materials such as SBA-15 should allow the deposition of thick coatings or even the formation of crystalline particles and rods inside the pore system. On the other hand, the pore system in SBA-15 is not interpenetrating as in MCM-48 and thus diffusion of the precursor into the pores is limited. The latter can lead to pore blocking before the pores are filled completely. Carbon infiltration of ordered mesoporous silica materials and subsequent dissolution of the host matrix is used for the preparation of ordered mesoporous carbon molecular sieves.[10,11] The carbothermal reduction of a carbon-containing mesoporous MCM-48 silica phase was also proposed as a new route to high-surface-area silicon carbide, even though the resulting material was not ordered on the mesoscopic scale.[12] Gas-phase infiltration techniques allow the controlled deposition of inorganic materials. Thus, direct SiC infiltration is a promising technique for the synthesis of well-defined composites or replication of the hosts mesopore system.

In the following, we describe the silicon carbide infiltration of MCM-48 and SBA-15 using gas-phase infiltration techniques. We will show that the deposition temperature can be used to control and direct the SiC nucleation inside or outside the pores. The deposition process is subsequently analyzed using nitrogen physisorption at 77 K, X-ray powder diffraction methods, and transmission electron microscopy. Dissolution of the silica matrix with HF etching affords porous high-surface-area SiC, but the degree of ordering of the pores is very low.

Experimental Section

MCM-48 Synthesis. For the synthesis of the host matrix, 0.56 g of KOH were dissolved in 22.32 g of distilled water in a 200-mL glass beaker. After 10 min, 4.74 g of the surfactant cetyltrimethylammonium bromide (CTAB, Acros, 99%) was added. The mixture was stirred for 20 min, and 4.17 g of tetraethyl orthosilicate (TEOS, Acros, 98%) was added to the solution at once. After 20 min, the white, milky product was transferred to a Teflon liner and placed into an autoclave for 3 days at 388 K. After cooling, the mixture was filtered and washed with 1500 mL of water. The filtered product was dried for 1 day at 363 K and then heated to 823 K for 5 h with a heating rate of 1 $Kmin^{-1}$.

SBA-15 Synthesis. $EO_{20}PO_{70}EO_{20}$ block copolymer (Pluronic P123, BASF, 4 g) was dissolved overnight in 105 mL of water (500-mL beaker) without stirring. The solution was then heated to 308 K and 20 mL of 37% HCl was added. After 10 min, 8.3 g of TEOS was added dropwise within 30 min (with stirring). The heating was continued for 4 h. The white solid was recovered by filtration but not washed with water. Thereafter, the product was immediately calcined at 823 K for 5 h (heating rate 1 $Kmin^{-1}$).

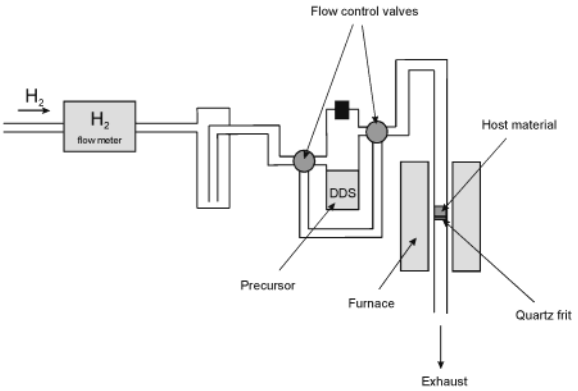

Figure 1. Chemical vapor infiltration system used for the SiC-infiltration.

Chemical Vapor Infiltration. The deposition of SiC was carried out at atmospheric pressure in a hot-wall vertical quartz tube reactor, 150 mm long and 12 mm in diameter (Figure 1). The mesoporous host (260 mg) was supported on a quartz frit located in the middle of the reactor.

Dimethyldichlorosilane (DDS, Fluka, 98%) was introduced into the reactor from a saturator using hydrogen as the carrier gas (2 Lh^{-1}). The molecular sieve was heated in hydrogen to 673 K with a heating rate of 10 $Kmin^{-1}$. Subsequently, the precursor was dosed into the reactor and the furnace was heated to the final deposition temperature.

Removal of the Silica Matrix. Mesoporous SiC was synthesized from SiC/SBA-15 nanocomposites by dissolution of the silica with HF. For this purpose, the infiltration was scaled-up in a hot-wall quartz tube reactor (30 mm i.d.) using 2.0 g of SBA-15 ($Ar/H_2 = 4:3$, $V = 2$ Lh^{-1}, DDS evaporation rate 1 mLh^{-1}, $T = 1118$ K). The composite was treated with 250 mL of 30% HF for 2 days, washed several times with distilled water, and dried at 90 °C.

Characterization. Wide-angle X-ray powder diffraction patterns were recorded in transmission geometry using a Stoe Stadi-P diffractometer and Cu $K\alpha_1$ radiation ($\lambda = 0.15405$ nm). Small-angle diffractograms were obtained on a Stoe Stadi-P θ/θ-diffractometer in the Bragg−Brentano (reflection) geometry using Cu $K\alpha$ radiation ($\lambda = 0.15418$ nm).

The nitrogen physisorption isotherms were measured at 77 K using a micromeritics ASAP 2010 apparatus. Prior to the measurements, the samples were evacuated at 473 K for 5 h. The specific surface area was calculated using the BET equation in a relative pressure range between $P/P_0 = 0.05-0.2$. The pore size distribution of the samples was determined from the desorption branch of the hysteresis loop of the isotherm, using the BJH formula assuming a cylindrical pore model.[13] The specific micropore volumes were estimated using t-plots.[14]

Transmission electron micrographs were obtained on a Hitachi HF 2000 TEM using a copper grid type sample holder. XPS measurements were carried out with a Kratos HSi instrument using a monochromated Al Kα (1486.5 eV) X-ray source operating at 300 W. A large sample area of 700 × 300 μm was probed. The pass energy for the narrow scans was set to 40 eV. The spectrometer was calibrated using Cu $2p_{3/2}$ and Au $4f_{7/2}$ peaks. The base pressure in the UHV chamber was $\leq 10^{-9}$ Torr. The spectra were charge referenced to the oxygen component set at a binding energy of 533 eV for O 1s. For the curve fitting, a nonlinear least squares curve fitting algorithm

(5) Lee, K. B.; Choi, C. S.; Oh, S. J.; Ri, H. C.; Cheon, J. *J. Phys. IV* **2001**, *11*, 481−486.
(6) Winkler, H.; Birkner, A.; Hagen, V.; Wolf, I.; Schmechel, R.; von Seggern, H.; Fischer, R. A. *Adv. Mater.* **1999**, *11*, 1444−1448.
(7) Parala, H.; Devi, A.; Rogge, W.; Birkner, A.; Fischer, R. A. *J. Phys. IV* **2001**, *11*, 473−479.
(8) Brieler, F. J.; Fröba, M.; Chen, L. M.; Klar, P. J.; Heimbrodt, W.; von Nidda, H. A. K.; Loidl, A. *Chem.-Eur. J.* **2002**, *8*, 185−194.
(9) Sauer, J.; Kaskel, S.; Janicke, M.; Schüth, F. *Stud. Surf. Sci. Catal.* **2001**, *135*, 315.
(10) Ryoo, R.; Joo, S. H.; Kruk, M.; Jaroniec, M. *Adv. Mater.* **2001**, *13*, 677−681.
(11) Vix-Guterl, C.; Boulard, S.; Parmentier, J.; Werckmann, J.; Patarin, J. *Chem. Lett.* **2002**, 1062−1063.
(12) Parmentier, J.; Patarin, J.; Dentzer, J.; Vix-Guterl, C. *Ceram. Int.* **2002**, *28*, 1−7.
(13) Barrett, E. P.; Joyner, L. G.; Halenda, P. P. *J. Am. Chem. Soc.* **1951**, *73*, 373−380.
(14) Rouquerol, F.; Rouquerol, J.; Sing, K. *Adsorption by Powders & Porous Solids*; Academic Press: San Diego, CA, 1998.

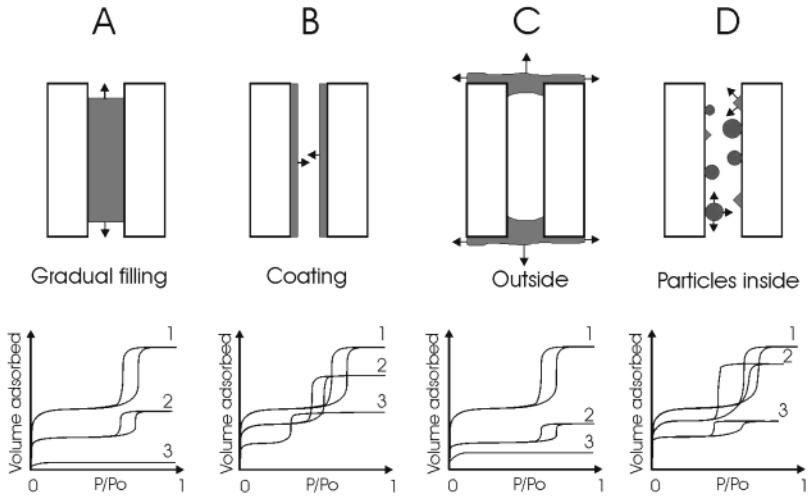

Figure 2. Models of pore-filling mechanisms for the gas-phase deposition in the presence of mesoporous molecular sieves and the corresponding nitrogen physisorption isotherms (curves: 1, starting material, 2 to 3, subsequent infiltration steps).

with a Gaussian−Lorentzian mix function and a Shirley background subtraction was applied.

Results and Discussion

Nitrogen Physisorption Method as an ex situ Monitoring Tool. Chemical vapor infiltration in the presence of porous materials can lead to the deposition of particles or coatings inside and outside the porous matrix. Several types of filling can be distinguished, the most important ones are gradual filling of the pores due to capillary condensation [Figure 2A], coating of the inner pore surface [Figure 2B], and particle formation inside the pores [Figure 2D]. The three different filling mechanisms are associated with distinguished changes of the corresponding nitrogen physisorption isotherms. Whereas gradual filling (A) causes a decrease of the overall sorption capacity but not a shift of the adsorption and desorption branch, the pore coating (B) results in a shift of the hysteresis adsorption and desorption branch toward lower relative pressures. In the case of particle formation (D), the shape of the hysteresis changes from H_1 to the H_2 type.[9,14]

Deposition outside the porous matrix [Figure 2C] is difficult to distinguish from gradual filling because the changes in the isotherm shape are comparable. These two mechanisms differ only in terms of integral specific mesopore volume with respect to the amount of material deposited. The specific mesopore volume, V_g, can be expressed as a function of weight gain (w) assuming an integral pore length, l, that does not change during the infiltration. This length, l, can be calculated from the specific pore volume of the porous silica matrix. For a pore filling model [Figure 2A, B, and D] at a maximum weight gain fraction w_{max}, the pore volume V_g becomes zero, as in eq 1

$$V_g = \frac{\pi\frac{d^2}{4}l - \frac{w \cdot m_{SiO_2}}{\rho_{SiC}}}{m_{SiO_2}(1+w)} \qquad (1)$$

where d = initial pore diameter; m_{SiO_2} = mass of SiO_2; ρ_{SiC} = density of SiC (3.2gcm^{-3}), and w = weight gain factor.

On the other hand, for deposition outside the matrix, without any pore blocking, the specific pore volume, V_g', will be zero only for infinite weight gain factors [eq 2].

$$V_g' = \frac{\pi\frac{d^2}{4}l}{m_{SiO_2}(1+w)} \qquad (2)$$

However, if pore closing is taken into account, the right side of eq 2 must be multiplied by the fraction of pores that remain open.

The idealized deposition mechanisms can be distinguished by means of nitrogen physisorption measurements and allow a detailed analysis of the deposition process in mesoporous molecular sieves. However, often more than one mechanism is observed, as some of the deposition processes outlined in Figure 2 take place in parallel. The relative contribution of the different deposition processes depends on the pore structure and diameter of the molecular sieve, the deposition temperature, precursor concentration, and flow rate.

SiC/MCM-48 Composites. We have studied the SiC chemical vapor infiltration (CVI) into MCM-48 for the manufacture of SiC/MCM-48 composites using chlorosilane precursors. The precursor, dimethyldichlorosilane (DDS), decomposes above 1023 K according to eq 3:

$$(CH_3)_2SiCl_2 \rightarrow SiC + 2\,HCl + CH_4 \qquad (3)$$

Hydrogen is used as a carrier gas. The reducing atmosphere also serves to suppress carbon formation. This process is heavily used for the fabrication of refractory SiC/SiC composites via infiltration of macroscopic woven SiC fiber architectures[15] but has not been used for the infiltration of ordered mesoporous materials before.

We have studied the SiC deposition at 1023 and 1163 K for the manufacture of SiC/MCM-48 nanocomposites. The temperature of the hot wall reactor can be used to adjust the deposition rate. In the following we show how the reaction temperature can be used to control the formation of the composite. The CVI process can thus

(15) Golecki, I. *Mater. Sci. Eng., R* **1997**, *20*, 37−124.

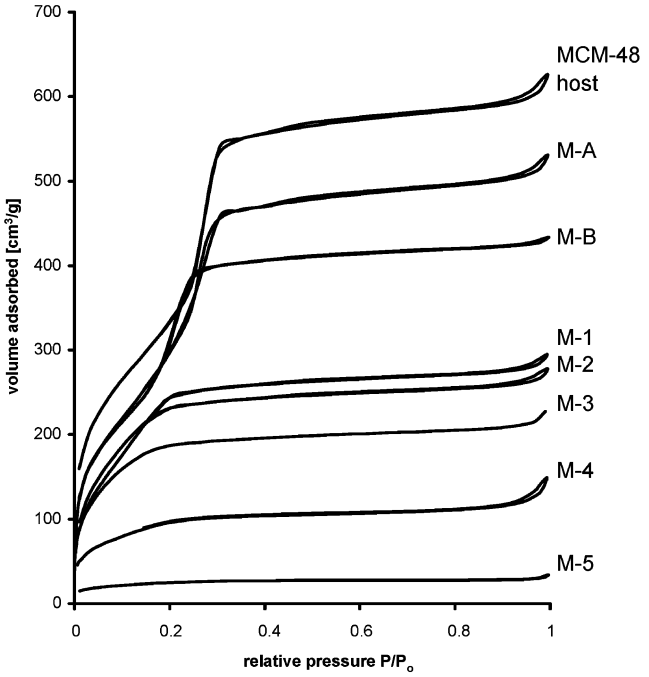

Figure 3. Nitrogen physisorption isotherms (77 K) of MCM-48 and SiC/MCM-48 composites obtained via chemical vapor infiltration. The sample codes correspond to the experimental parameters listed in Table 1.

Table 1. Experimental Parameters for the Synthesis of SiC/MCM-48 Nanocomposites

sample	T [K]	t [h]	r[a] [mLh^{-1}]	V_g [cm^{3}g^{-1}]
MCM-48				1.04[b]
M-A	1023	6.0		0.95[b]
M-B	1163	6.0		0.84[b]
M-1	1023	2.0	4.0	0.35[c]
M-2	1023	4.5	4.2	0.33[c]
M-3	1023	6.0	5.0	0.29[c]
M-4	1163	3.0	2.3	0.14[c]
M-5	1163	6.0	3.2	0.04[c]

[a] r = DDS evaporation rate. [b] V_g = specific mesopore volume (BJH method). [c] V_g = specific micropore volume (t-plot method).

be used to produce either a thin coating on the inner surface of the porous matrix at low deposition temperatures or a thicker coating on the outer surface of the porous particles leading to a protective coating.

SiC Infiltration at 1023 K. A short infiltration time of 2 h is sufficient to achieve a detectable degree of infiltration into the MCM-48 host system. Nitrogen physisorption measurements allow estimating the amount of material deposited and the thickness of the coating (Figure 3). For the host system MCM-48 a characteristic steep adsorption branch at $P/P_0 = 0.3$ is observed due to the capillary filling of the mesopores. The host has a narrow pore size distribution and a pore diameter of 2.4 nm. After 2 h infiltration at 1023 K (Table 1, sample M-1), instead of the steep branch, a type I isotherm is observed. Thus, the pore size is reduced to $d < 2$ nm. The shape of the isotherm at $0.05 < P/P_0 < 0.2$ indicates a significant contribution of secondary micropores.[14] At the same time, the overall adsorption capacity decreases as expected for a reduction in the specific pore volume associated with the infiltration process. For longer infiltration times (M-2 and M-3) the adsorption step is subsequently shifted toward lower relative pressures and the pore volume

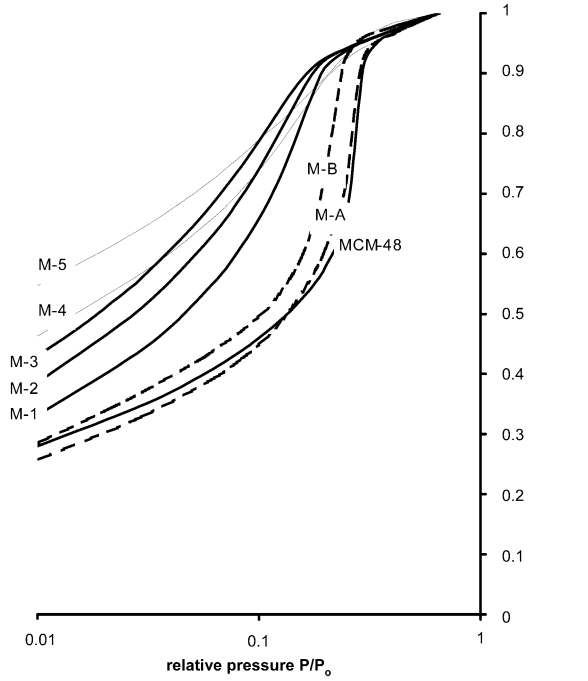

Figure 4. Logarithmic plot of the normalized nitrogen physisorption isotherms (77 K). The sample codes correspond to the experimental parameters listed in Table 1. Broken lines are used for isotherms of samples heat treated without precursor (A, 1023 K; B, 1163 K), solid lines are for samples infiltrated at 1023 K, and thin lines are for samples infiltrated at 1163 K.

subsequently decreases which indicates the formation of a thin coating on the inner pore wall. Pore size analyses in the micropore regime are difficult because they rely on pore models and known interaction potentials between the adsorbate and the pore wall.[14] Little is known about the surface potential of hard ceramics such as SiC. Thus, pore size analyses in the micropore regime using DFT or Horvath−Kawazoe methods do not allow the calculation of the exact pore size. However, the relative change of the pore size can be analyzed in logarithmic plots of normalized physisorption isotherms.[16,17] They allow a comparison of pore sizes of materials that are comparable in surface composition. The decrease of the pore size with increasing infiltration time can thus be identified by comparing the relative pressure at which the nitrogen adsorption occurs. The logarithmic plot of the adsorption isotherms for composites synthesized at 1023 K shows that the inflection points move toward decreasing relative pressure with increasing infiltration time indicating a decrease in the pore size with increasing infiltration time (M-1−M-3, solid lines, Figure 4). In contrast, the heat treatment alone (M-A) in hydrogen does not cause a significant change of the pore size.

Small-angle XRD patterns of the infiltrated materials (Figure 5) show that the three-dimensional ordered pore arrangement remains intact even after an infiltration period of 6 h (M-3). The (211) and the (220) peak of the cubic mesoporous host matrix are still present but the (420) and (332) reflection have vanished indicating a

(16) Farrusseng, D.; Schlichte, K.; Spliethoff, B.; Wingen, A.; Kaskel, S.; Bradley, J. S.; Schüth, F. *Angew. Chem., Int. Ed.* **2001**, *40*, 4204−4207.
(17) Saito, A.; Foley, H. C. *Microporous Mater.* **1995**, *3*, 531−542.

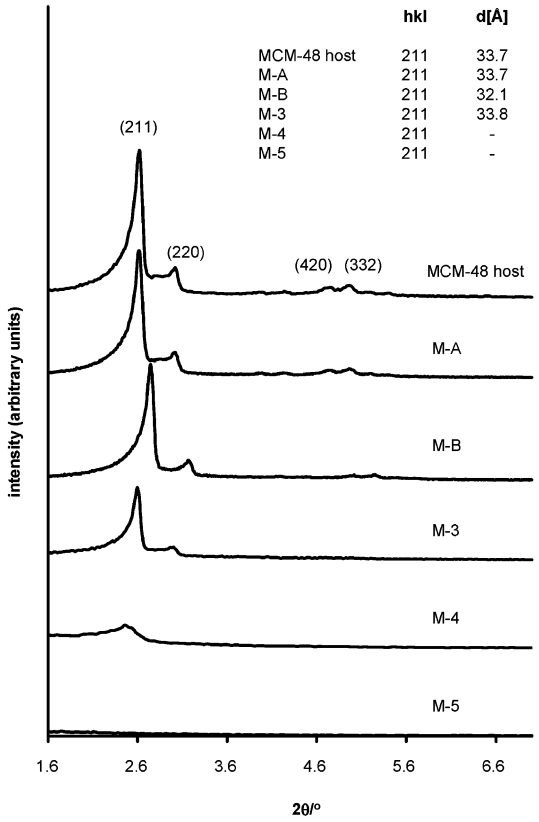

Figure 5. Small-angle X-ray diffraction powder patterns of the MCM-48 host matrix and the SiC/MCM-48 composite materials.

lower degree of ordering as compared to the host matrix. The latter could be caused by a loss of organization on the mesoscopic scale or is a consequence of the infiltration, as a nonuniform deposition inside the pores will lead to a loss of translation symmetry. In fact, a somewhat nonuniform coating is also in agreement with the logarithmic plots of the adsorption isotherms because the adsorption step is not as steep as compared to that of the host material. Another reason for the reduced intensity could be the decrease of the contrast between the filled pores and the pore walls or the formation of small domains with different orientation. The positions of the reflections in the small-angle XRD patterns do not change with prolonged infiltration. Thus, the mesoscopic lattice constant is not changed. For example the (211) reflection of the host matrix is located at 33.7 Å and that of the sample M-3 is at 33.8 Å. Thus, the reduction in pore size is not caused by a matrix collapse or shrinkage of the pore system. The intact structure of the mesoscopic pore arrangement is also observed in transmission electron micrographs (Figure 6). A comparison of the cubic matrix (Figure 6a) with the SiC/MCM-48 composite (Figure 6b) shows only a slight variation of the contrast between the empty pores and the pore walls, probably caused by the infiltration of SiC. Whereas in hexagonal mesoporous materials the observation of the infiltrated component can be achieved by imaging along the 6-fold axis,[9,18] the cubic interwoven network structure of MCM-48 does not allow for the direct visualization of the coating. The pore volume decreases from 1.04 cm^3g^{-1} in the host material to 0.29 cm^3g^{-1} after 6 h infiltration (M-3). The experimental weight gain is 74%. If all the deposited silicon carbide were inside the pores in the form of SiC with a density of 3.2 gcm^{-3}, the specific pore volume should be reduced to only 0.47 cm^3g^{-1}. This discrepancy could be due to pore blocking, additional deposition on the outer surface, limitations of the t-plot and BJH method for the pore volume estimation, or because the density of the deposited material is lower as compared with that of bulk silicon carbide.

We could not detect significant deposition of SiC outside the pore system in the TEM studies. The macroscopic spherical morphology of the MCM-48 particles also remains intact after infiltration. The combined results of the physisorption, XRD, and TEM results confirm that the deposition occurs mainly inside the pores. Thus, at 1023 K deposition on the outer surface of the spherical particles leading to pore blocking and closing seems to be negligible.

Samples infiltrated at 1023 K (M-1, M-2, and M-3) do not show reflections in wide-angle X-ray diffraction patterns. Neither cubic SiC nor any other modification of SiC is detected by means of wide-angle X-ray diffraction. The material deposited could thus be either X-ray amorphous or the small domain (crystallite) size is causing an increased peak broadening. The X-ray amorphous character of ultrathin coatings is not uncommon for materials synthesized on the inner surface of ordered mesoporous materials.[18] The SiC formation is also detected in IR spectra. Pure SiC typically shows a broad band centered at 840 cm^{-1} that is attributed to the Si−C fundamental vibrations. However, some deviations are found depending on the preparation conditions.[19] Pure MCM-48 shows a weak absorption at 805 cm^{-1}. Gradual formation of the thin SiC layer by CVI at low temperature (M-3) shows a broadened band centered at 809 cm^{-1} that is significantly increased in intensity due to the superposition of the Si−C (840 cm^{-1}) and Si−O vibrations. A more in-depth analysis of the interfacial chemical composition will be discussed along with SBA-15 infiltration by means of XPS and ^{29}Si MAS NMR.

SiC Infiltration at 1163 K. An increase of the deposition temperature increases the deposition rate. The rapid pore filling can be monitored using nitrogen physisorption techniques. The steep adsorption branch of the isotherm is lost and the isotherms of the infiltrated samples are of type I (M-4 and M-5, Figure 3). The height of the plateau is a direct measure of the amount of SiC deposited, because the addition of a dense material causes a decrease in the specific pore volume, no matter whether the material is deposited inside or outside the porous matrix. Thus, the isotherms clearly demonstrate the enhanced deposition rate for the samples M-4 and M-5 (Figure 3) as compared to the samples obtained at 1023 K (M-1 to M-3). Whereas at 1023 K the micropore volume decreases to 0.29 cm^3g^{-1} after 6 h of infiltration, in contrast, at 1163 K the volume decreased to only 0.04 cm^3g^{-1} even though a lower evaporation rate was used. However, TEM studies (Figure 6) also reveal the deposition of 20−30-nm-sized

(18) Sauer, J.; Marlow, F.; Spliethoff, B.; Schüth, F. *Chem. Mater.* **2002**, *14*, 217−224.

(19) Vix-Guterl, C.; Alix, I.; Gibot, P.; Ehrburger, P. *Appl. Surf. Sci.* **2003**, *210*, 329−337.

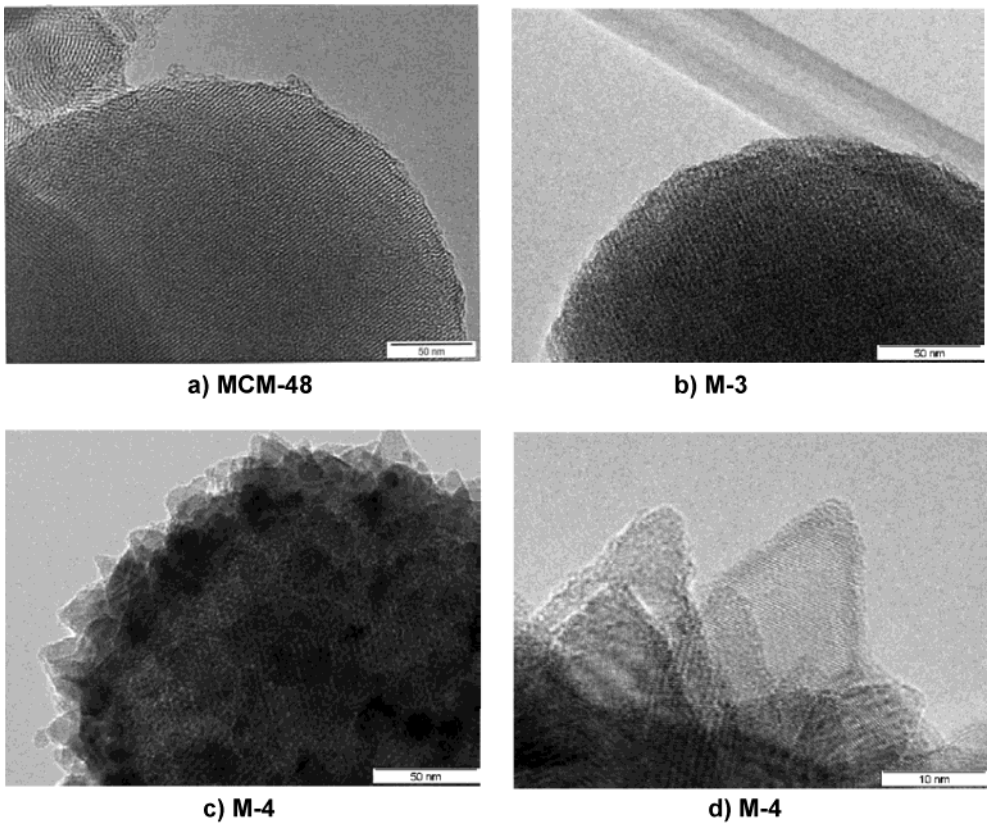

Figure 6. Transmission electron micrographs of the mesoporous host matrix (a) and the SiC/MCM-48 nanocomposites (b−d) synthesized via infiltration at 1023 K (b) and 1163 K (c and d).

SiC particles on the outer surface of the spherical particles (Figure 6c and d). Thus, not only are the pores filled, causing the reduction in pore size and specific pore volume, but the composites are also covered with a hard protective shell on the outer surface. Logarithmic plots of the isotherms (Figure 4, M-4 and M-5) show that the resulting pores are smaller as compared with materials obtained at 1023 K but also the pore size distribution is broad and the nitrogen uptake covers a wider range. The latter indicates a less uniform coating on the inner surface area. An enhanced deposition of SiC at the entrance of the channels near the outer surface of the matrix could also cause pore closing and thus initiate SiC formation on the outer surface because, in that case, for the precursor the access to the inner surface is blocked. The observed mass gains for the samples M-4 and M-5 are 131% and 515%, respectively. Assuming a complete filling of the mesopores with silicon carbide ($\rho = 3.2$ gcm^{-3}) would allow a maximum weight gain of 334%. Thus, in M-5 not only are the pores filled but deposition outside the host material is significant. For sample M-4 the micropore volume of 0.14 cm^{3}g^{-1} should correspond to a weight increase of 192% if only the pores are filled, which is significantly higher than the experimental weight gain of 131%. Thus, at higher temperature, in addition to the pore filling, a significant amount of silicon carbide leads to blocking of the pores.

On the other hand, the ordered mesoporous host system is still intact as can be seen on the transmission electron micrographs (Figure 6c). The ordered pore system is also detected in small-angle X-ray diffractograms, at least for the short infiltration period (Figure 4, M-4). Because the small-angle reflections originate from the contrast between the pore walls and the empty pores, the intensity of the small-angle reflections typically decreases with pronounced infiltration as long as the density of the infiltrated component is comparable to that of the host system.[20]

The SiC nanoparticles, 20−30 nm in diameter, are also detected using wide-angle X-ray diffraction. The main product can be assigned to cubic β-SiC[12] but some broad peaks close to the (111) reflection indicate the simultaneous presence of other SiC polytypes.

The SiC nanoparticles on the outer surface are typically 20−30 nm in diameter and form a hard protective shell of the porous particle. The resulting core−shell particles represent a remarkable new element in the development of nanocomposites. They are ordered porous materials composed of a rather soft matrix (silica) that is protected by an ultrathin, extremely hard, nanoscopic coating of SiC crystallites on the outer surface resulting in a hedgehog-like appearance of the nanocomposite particles (Figure 6c). The latter could be valuable for applications of ordered mesoporous materials under severe abrasive or corrosive conditions.

SiC/SBA-15 Composites. *Thermal Stability of the Host and Effect of Deposition Parameters.* The thermal stability of the host material SBA-15 is typically limited to temperatures up to 1243 K.[21−23] The heat treatment causes a significant shrinkage and reduction of the BET surface area. However, the stability also depends on the synthesis conditions and the presence of water. At

(20) Sauer, J.; Marlow, F.; Schüth, F. *Phys. Chem. Chem. Phys.* **2001**, *3*, 5579−5584.

Table 2. Parameters for the Chemical Vapor Infiltration of SBA-15 and Results of the Nitrogen Physisorption Experiments and Small Angle X-ray Powder Patterns (Deposition Temperature 1118 K)[a]

sample	t [h]	r [mLh^{-1}]	S_g [m^{2}g^{-1}]	V_g^{meso} [cm^{3}g^{-1}]	V_g^{micro} [cm^{3}g^{-1}]	w [%]	d_{pore} [Å]	d_{100} [Å]
SBA-15 host			500	0.463	0.079		45.1	86.8
SA-1	2.5	0	394	0.422	0.036		43.6	83.1
SA-2	4.5	0	320	0.353	0.017		42.0	80.2
SA-3	0.0	0.7	312	0.352	0.016	34	42.5	86.8
SA-4	3.5	0.8	173	0.100	0.005	77	30.4	86.5
SA-5	5.0	0.3	165	0.165	0.000	50	36.5	86.5
SA-6	5.5	0.9	80	0.028	0.016	111	26.6	86.6

[a] r = DDS evaporation rate; S_g = BET surface area; V_g^{meso} = mesopore volume calculated from the desorption branch (for the pore size between 20 and 80 Å); V_g^{micro} = micropore volume calculated using the t-plot method; d_{pore} = average mesopore diameter; d_{100} = (100) d spacing.

higher temperatures, collapse of the pores is observed. Because the deposition temperature used in our experiments is close to this limiting temperature, and because of variations in the thermal stability depending on the synthesis conditions, it was necessary to perform blank experiments in which the host material was exposed to the deposition temperature and carrier gas but without introducing the molecular precursor [Table 2; SA-1 and SA-2].

At temperatures close to 1243 K, typically a slow shrinkage of the three-dimensional pore structure is observed, leading to a decreasing surface area and pore size.[21] After treating the pure SBA-15 host in H_2 at 1118 K for 4.5 h [Table 2; SA-2] the (100) reflection of the SBA-15 host is shifted from d_{100} = 86.8 Å (Table 2; SBA-15 host) to 80.2 Å [Figure 7]. Thus, at the deposition temperature, the host material contracts as long as no precursor is introduced. Nitrogen physisorption isotherms confirm the shrinkage [Figure 8]. With increasing duration of the heat treatment, the specific surface area decreases from 500 to 320 m^{2}g^{-1} [Table 2] and the average pore diameter (calculated from the desorption branch) decreases from 45.1 to 42.0 Å [Table 2; SA-2]. The micropore volume of the SBA-15 host material (V_g = 0.079 cm^{3}g^{-1}) decreases gradually to 0.036 cm^{3}g^{-1} (SA-1) and to 0.017 cm^{3}g^{-1} (SA-2). Thus, closing of the micropores, present in the mesopore walls, is probably the reason for the shrinkage of the three-dimensional pore system of SBA-15 in the early stages. The latter causes densification of the silica walls and a decrease of the measured pore diameter and d spacing.[21]

In contrast to the samples heat treated without DDS precursor, which show significant shrinkage of the pore system and a reduced d_{100} spacing, for samples exposed to the DDS precursor at the same temperature (1118 K), the d_{100} spacing does not change more than 0.5 Å [Figure 9]. With prolonged infiltration, using high precursor concentrations, the (110) and (200) peak intensity decreases, and, after 5 h, the higher order peaks disappear. Thus, the degree of two-dimensional ordering in the host material is disturbed. The reason is the deposition of SiC inside the pores that is not uniform enough to maintain the periodicity of the mesopore structure. Even for very

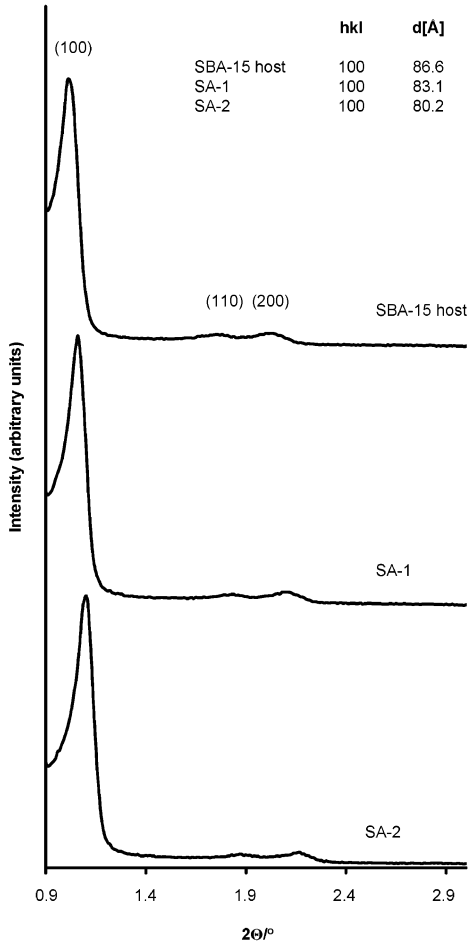

Figure 7. Small-angle X-ray diffraction patterns of SBA-15 and thermally treated SBA-15 [Table 2].

short infiltration periods (SA-3 sample), the pore size decreases from 45.1 to 42.5 Å without changing the distance of (100) planes. Longer infiltration causes a significant decrease of the pore size as deduced from the desorption branch [Figure 10]. The mesopore size decreases from 45.1 Å in the host to only 26.6 Å after 5.5 h infiltration, whereas in the thermal treatment without precursor, the pore size is reduced to only 42.0 Å [Table 2]. The micropore volume is reduced from 0.079 to 0.016 cm^{3}g^{-1} suggesting deposition inside the micropores of the SBA-15 mesopore walls in the early stages of infiltration.

Even the shortest infiltration period (SA-3) causes a reduction of the specific mesopore volume, V_g, from 0.463 to 0.352 cm^{3}g^{-1}. Assuming a filling of the mesopores inside the channels, without any deposition taking place outside the host material, such a reduction of V_g

(21) Shin, H. J.; Ryoo, R.; Kruk, M.; Jaroniec, M. *Chem. Commun.* **2001**, 349−350.
(22) Galarneau, A.; Desplantier-Giscard, D.; Di Renzo, F.; Fajula, F. *Catal. Today* **2001**, *68*, 191−200.
(23) Cassiers, K.; Linssen, T.; Mathieu, M.; Benjelloun, M.; Schrijnemakers, K.; Van Der Voort, P.; Cool, P.; Vansant, E. F. *Chem. Mater.* **2002**, *14*, 2317−2324.

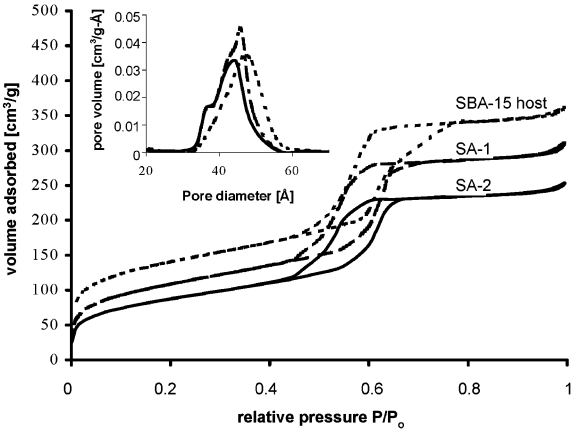

Figure 8. Nitrogen physisorption isotherms (77 K) and pore size distribution of SBA-15 and thermally treated SBA-15 [Table 2].

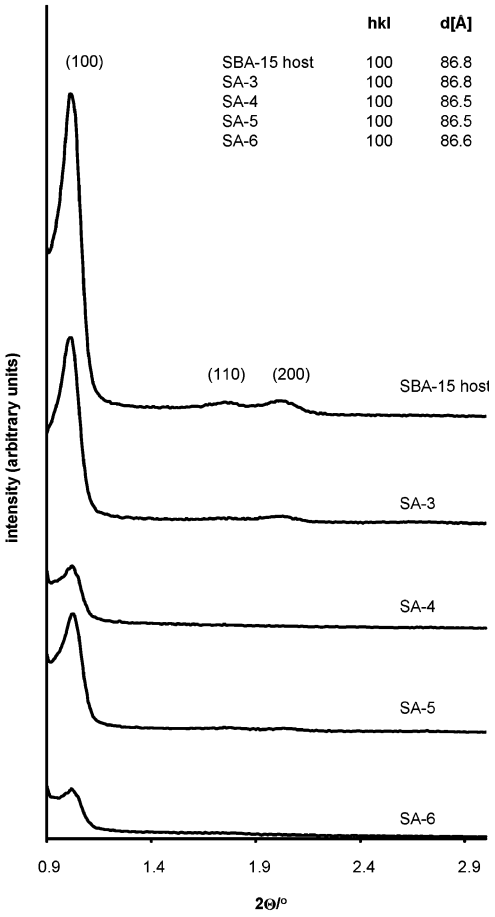

Figure 9. Small-angle X-ray diffraction patterns of SBA-15 and infiltrated SBA-15 [Table 2].

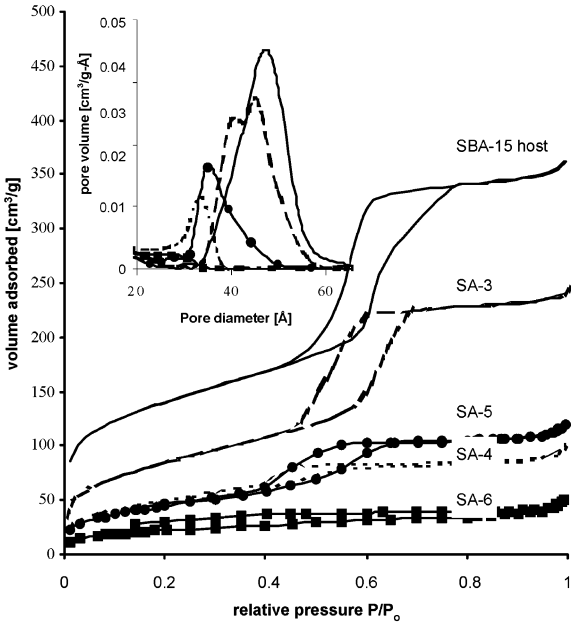

Figure 10. Nitrogen physisorption isotherms (77 K) and pore size distribution of SBA-15 and infiltrated SBA-15.

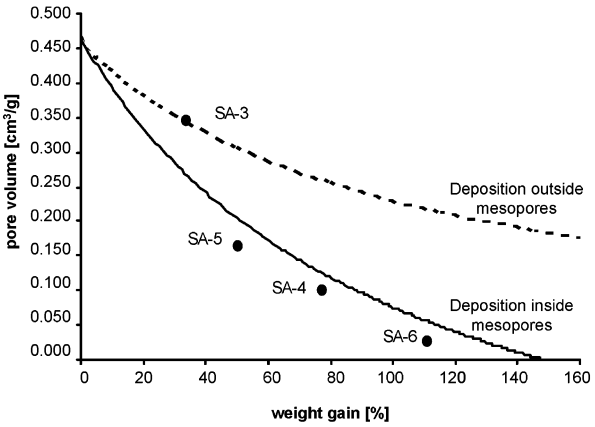

Figure 11. Specific mesopore volume calculated as a function of the weight gain (w): solid line, eq 1; broken line, eq 2.

Table 3. Comparison of the Measured Specific Pore Volumes and Diameters with Calculated Values Assuming the Pore Coating Model [Figures 11 and 12][a]

sample	w [%]	$V_{g,exp}$ [cm^3g^{-1}]	$V_{g,calc}$ [cm^3g^{-1}]	$V_{g,exp}/V_{g,calc}$ [%]	d_{exp} [Å]	d_{calc} [Å]	d_{exp}/d_{calc} [%]
SA-3	34	0.352	0.266	132	42.5	39.6	107
SA-4	77	0.100	0.124	81	30.4	31.3	97
SA-5	50	0.165	0.204	81	36.5	36.7	99
SA-6	111	0.028	0.056	50	26.6	22.6	118

[a] V_g = specific mesopore volume; d = average mesopore diameter.

would correspond to a weight gain of 17% [eq 1, Figure 11]. However, the experimental weight gain is much higher (34%, Table 3) indicating either deposition on the outer surface of the porous particles or inside the micropores of the pore walls. The latter is reasonable, as the specific micropore volume decreases substantially. A further decrease of the pore size to 30.4 Å (SA-4) is observed after 3.5 h infiltration, whereas with a lower precursor evaporation rate, the pores are larger (36.5 Å, SA-5) after 5 h.

For these samples, the specific pore volume is lower than expected from the weight gain for a pure infiltration model inside the pores (gradual, coating, or particle filling). For SA-4 and SA-5, the measured mesopore volume is 81% of the calculated volume. The latter could be due to a lower density of the deposited material, for example in the case of oxycarbide formation, or due to pore blocking and enhanced deposition outside the pores [Figure 11].

A pronounced decrease of the size of mesopores to only 26.6 Å (SA-6) is observed after 5.5 h infiltration. The pore size distribution is very broad and does not show a maximum value [Figure 10]. The pore diameter after infiltration, d_I, can be expressed as a function of weight

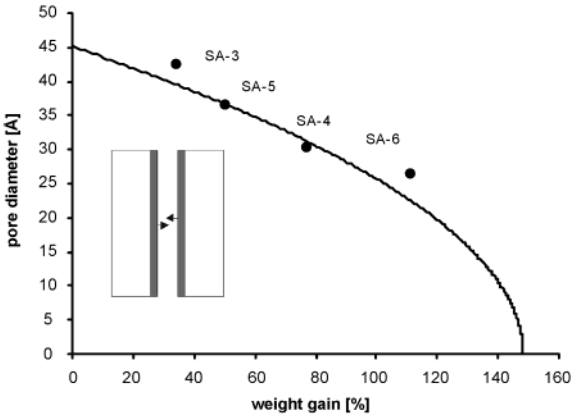

Figure 12. Pore diameter calculated as a function of weight gain: solid line, pore coating model (eq 4).

gain, w, assuming a pore coating model [Figure 2, B; eq 4].

$$d_{\mathrm{I}} = \sqrt{\frac{4}{\pi l}\left(\frac{\pi d^2}{4} l - \frac{w \cdot m_{\mathrm{SiO_2}}}{\rho_{\mathrm{SiC}}}\right)} \qquad (4)$$

For SA-4 and SA-5, the experimental pore size is close to the expected value [Figure 12, Table 3]. On the other hand, for the short infiltration (SA-3) the observed pore size is larger which is in agreement with the initial filling of micropores in the beginning of the infiltration. For long-term infiltration, the pore size is also larger than expected, indicating a significant degree of deposition on the outer surface of the matrix.

For SA-6, an increase in the micropore volume to 0.016 cm^3g^{-1} is observed compared to SA-4 and SA-5 indicating inhomogeneous pore coating or even particle formation inside the pores leading to micropore formation.

Thus, three stages of infiltration can be distinguished. In the early stages during the heat up of the infiltration setup, micropore filling leads to an increased stability of the pore walls, and thus shrinkage of the pore system − as observed for the pure heat treatment − is avoided. For longer infiltration periods, coating of the inner pore walls is observed but as a competing process, deposition outside the pores and pore blocking occurs. Further infiltration, leading to a decrease of the pore diameter below 30 Å, is less uniform and the resulting pore size distribution is very broad. Thus, access of the precursor becomes more and more hindered inside the smaller pores and leads to pore closing.

In wide angle XRD powder patterns, crystalline SiC is detected only after at least 3.5 h of infiltration (SA-4 and SA-6) using higher precursor evaporation rates. The other samples were X-ray amorphous. The Bragg reflections can be assigned to cubic β-SiC. The asymmetric shape of the (111) reflection indicates the presence of a small impurity of SiC polytypes.

However, the SiC particles in samples containing crystalline SiC are mostly present on the outer surface of SBA-15. They are discerned in transmission electron micrographs of sample SA-4 [Figure 13]. Whereas the SBA-15 host material shows a high contrast between the empty pores and the silica pore walls [Figure 13a], in the infiltrated sample the contrast is reduced and a particulate coating on the outer surface is observed

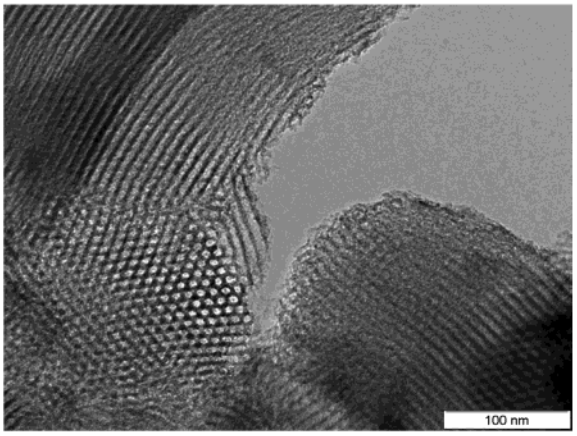

(a) SBA-15(A) host

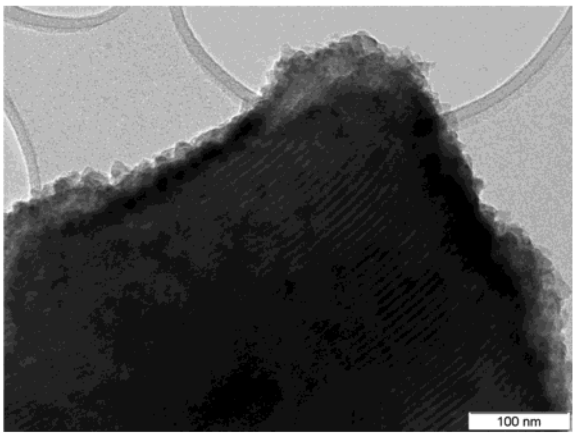

(b) SA-4 sample

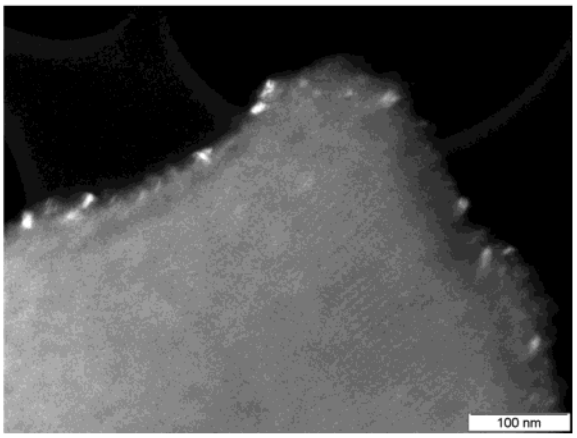

(c) dark field image of SA-4 sample

Figure 13. Transmission electron micrographs of SBA-15 (a) and the infiltrated SA-4 sample (b and c).

[Figure 13b] that contains the crystalline particles. The crystallites were identified using dark field imaging [Figure 13c]. The inner pore coating, proposed from the sorption analyses, cannot be seen because of the low contrast between SiC and SiO_2.

Thus, chemical vapor infiltration of SiC into SBA-15 allows the manufacture of SiC/SBA-15 composites. However, only thin and X-ray amorphous coatings on the inner pore walls are obtained, whereas longer infiltration procedures result in significant deposition of SiC on the outer surface and thus a dense and hard

Table 4. Parameters for the Chemical Vapor Infiltration of SBA-15 (Deposition temperature 1118 K, DDS evaporation rate 0.2 mLh^{-1})

sample	*t* [h]	w [%]
SBA-15 host		
SB-1	3.5	28
SB-2	5.0	46
SB-3	6.0	87
SB-4	9.0	102

coating is obtained that causes blocking of the pore entrances.

Gradual Growth of Crystalline Silicon Carbide. To maximize the amount of inner pore coating versus deposition outside the pores, a more gradual filling was studied using a lower evaporation rate (0.2 mLh^{-1}) [Table 4]. Using wide angle XRD powder patterns, crystalline SiC is detected after 5−6 h of infiltration. They are comparable to the samples prepared with higher precursor concentrations but the reflections are broader. A longer time of deposition (SB-3) results in a material with a broad peak at 36°(2θ). The intensity of the reflection increases with increasing duration of the infiltration (SB-4). The peak can be assigned to the (111) reflection of β-SiC. As compared to SA-4 and SA-6, prepared using higher precursor concentrations, the peak width is significantly enhanced indicating smaller crystallites.

Because of the X-ray amorphous character of the coating, information from diffraction is limited. To get a deeper insight into the composition and structure of the coating formed in the course of the infiltration, X-ray photoelectron spectroscopy (XPS) was used to characterize each sample. XPS allows detection of a gradual change in the composition with increasing duration of the infiltration. Even though XPS is a surface analysis tool, and the maximum penetration depth is only 50 Å, it can provide information for porous materials with domain sizes of only a few nanometers.

Both Si 2p and C 1s signals provide information about the composition of the infiltrated component. Four different species were identified in the Si 2p spectra [Figure 14, Table 5].

Short infiltration produces only a small amount of SiC (SB-1). The main contribution is assigned to the SiO_2 pore walls, but, in addition to SiC, significant portions of the peak can be assigned to elemental silicon and silicon oxycarbide. The latter is here denoted as SiO_xC_y as it is a mixture of SiO_3C-, SiO_2C_2-, and $SiOC_3$- species with a peak position located between SiO_2 and SiC.[24] Even though it is difficult to attribute the asymmetric shape of the Si 2p signal for SB-1 to the presence of SiO_xC_y, and the data should not be over-interpreted in terms of quantification, the profile fitting is significantly improved if this species is taken into account. For longer infiltration periods, the formation of SiO_xC_y and SiC is even more pronounced and separate maxima for SiO_2 and SiC are observed after 9 h infiltration.

Silicon oxycarbide formation in the early stages of the infiltration (SB-1) is also confirmed in the C 1s spectra [Figure 15]. The SiO_xC_y/SiC ratio is 2.7 and comparable to the ratio estimated from the Si 2p spectra (3.6). A small signal at 281 eV could not be assigned to any

(24) Onneby, C.; Pantano, C. G. *J. Vac. Sci. Technol., A* **1997**, *15*, 1597−1602.

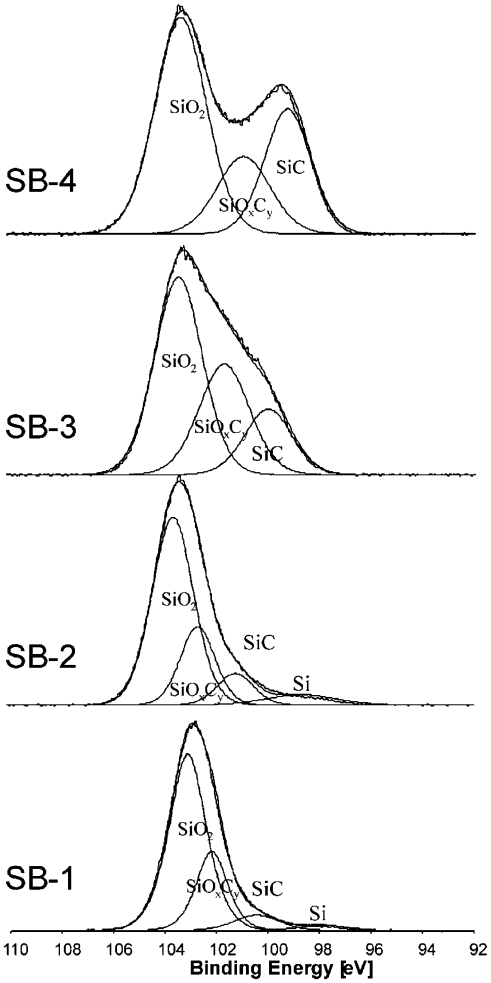

Figure 14. High-resolution Si 2p X-ray photoelectron spectra of the gradually infiltrated SBA-15 samples [Tables 4 and 5].

Table 5. Relative Intensities of the Si 2p and C 1s Peaks (XPS)

species	SB-1 at. % (eV)	SB-2 at. % (eV)	SB-3 at. % (eV)	SB-4 at. % (eV)
Si2p SiO_2	66 (103.1)	63 (103.6)	52 (103.4)	53 (103.3)
Si2p SiO_xC_y	25 (102.2)	22 (102.6)	31 (101.6)	20 (100.9)
Si2p SiC	7 (100.4)	9 (101.2)	17 (100.0)	28 (99.2)
Si2p Si	2 (97.9)	7 (98.7)		
C1s C−C, C−H	26 (284.4)	21 (284.8)	18 (284.8)	14 (284.3)
C1s SiO_xC_y	49 (283.3)	46 (283.7)	37 (283.8)	28 (282.9)
C1s SiC	18 (282.2)	23 (282.5)	45 (282.8)	58 (281.6)
C1s	7 (280.9)	10 (281.0)		

known compound present in the system. Only after 6 h infiltration is the SiC/SiO_xC_y ratio close to 1.0 (SB-3). In the C 1s spectra of SB-3, differentiation of SiC and SiO_xC_y is possible. On the other hand, small amounts of carbon deposits (C−C, C−H; 284.3−8 eV) are also detected in the C 1s spectra. Carbon deposition is especially favored for low hydrogen concentration, whereas too high hydrogen concentration can cause the deposition of elemental silicon. However, with increasing degree of deposition the relative contribution of the C−C peak decreases.

The XPS measurements suggest that the interfacial coating of the surface is composed of silicon oxycarbide, forming in a reaction of the precursor with the silica walls. Silicon carbide grows on this interface with particle sizes of only a few nanometers that are barely detected using X-ray powder diffraction methods. Silicon

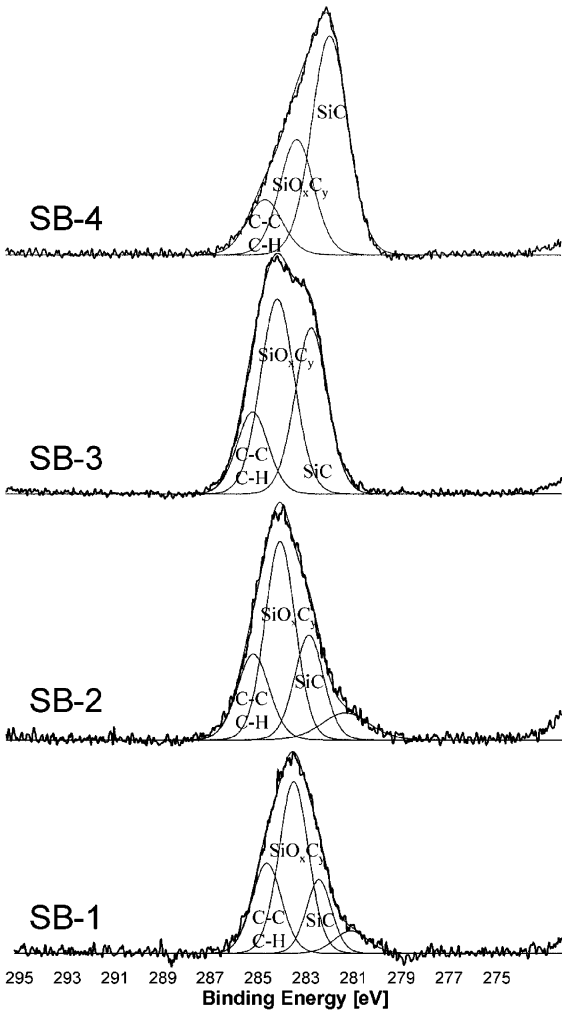

Figure 15. C 1s X-ray photoelectron spectra of gradually infiltrated SBA-15 materials [Tables 4 and 5].

oxycarbides were also detected in the surface oxidation of silicon carbide.[24] In this case the oxycarbide forms a stable interface between SiC and the outer SiO_2 coating.

Mesoporous SiC via Dissolution of Silica from the SiC/SBA-15 Composite. An indirect method to prove the infiltration is dissolution of the silica matrix of the composite. In this way, ideally, an inverse replica of the host system should be obtained. The latter has been shown for carbon materials by Ryoo et al. using MCM-48 as well as SBA-15.[10,21,25] If the pore system is interconnected, an inverse free-standing replica of the pore system is obtained. In the case of SBA-15, interconnection is realized through micropores that can be present depending on the synthesis conditions.

We have used a SiC/SBA-15 composite obtained through 1 h 40 min infiltration (30% weight gain) with a specific pore volume, decreased from 0.7 to 0.25 cm^3g^{-1} and a residual specific surface area of 294 m^2g^{-1}. After dissolving the silica, the specific pore volume increased from 0.25 to 0.96 cm^3g^{-1} which is even higher than that of the host SBA-15 (0.7 cm^3g^{-1}). The specific surface area increased from 294 m^2g^{-1} (SiC/SBA-15 nanocomposite) to 508 m^2g^{-1} (mesoporous SiC) [Figure 16]. However, the pore size distribution of the dissolved

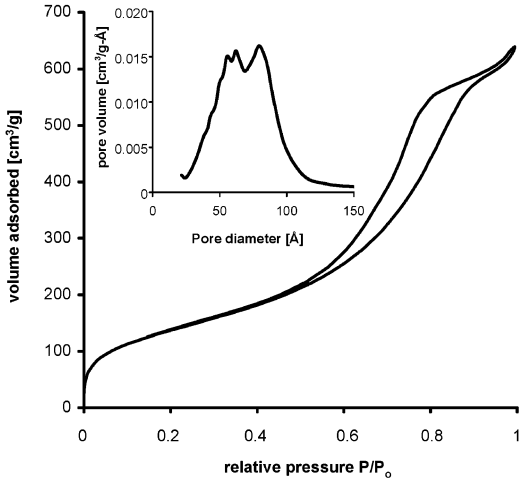

Figure 16. Nitrogen physisorption isotherm (77 K) and pore size distribution of the high-surface-area SiC obtained via silica removal from the SiC/SBA-15 composite.

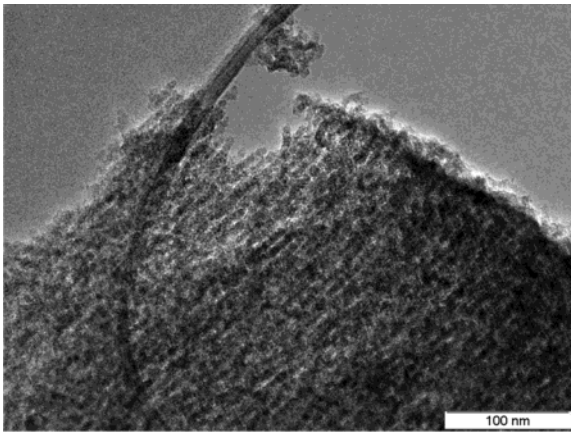

Figure 17. Transmission electron micrograph of the high surface area SiC obtained via silica removal from the SiC/SBA-15 composite.

sample is not as narrow as that of SBA-15. The mesoporous SiC does not show long range order of the nanotubes in small-angle X-ray diffractograms. ^{29}Si MAS NMR spectra confirm the absence of SiO_2. The broad NMR signal of the SiC is centered at −8 ppm and covers a range between −30 and 10 ppm which is typical for amorphous SiC.[26] In addition, SiC_xO_y species are detected: $SiCO_3$ at −61 ppm, SiC_2O_2 at −30 ppm, and SiC_3O at 15 ppm. However, the lower intensity of these signals indicates a low concentration of silicon oxycarbide in the material. The Si 2p X-ray photoelectron spectra give similar results with two contributions in the signal: one at 100.3 eV (SiC, 59% at.) and another at 101.8 eV (SiO_xC_y, 41% at.). However, quantitative differentiation between the carbide and oxycarbide is difficult by means of XPS due to the overlap of the peaks. An elemental analysis of the mesoporous SiC shows 25.5% carbon which is only slightly lower than that expected for pure SiC (30% C). Transmission electron micrographs reveal the morphology of the mesoporous SiC [Figure 17]. Ideally, inverse replication after deposition of a thin coating should give SiC tubes, interconnected through rods that result from the filled

(25) Joo, S. H.; Jun, S.; Ryoo, R. *Microporous Mesoporous Mater.* **2001**, *44*, 153−158.

(26) Roewer, G.; Herzog, U.; Trommer, K.; Müller, E.; Frühauf, S. In *Structure & Bonding*; Jansen, M., Ed.; Springer: Berlin, 2002.

micropores. The detected morphology [Figure 17] is different from that picture. Instead, the particles are connected into strings that are more or less aligned in one direction to form a poorly ordered array of nanorods. Whereas carbon materials are resistant against HF etching, it must be questioned whether the small domains of silicon oxycarbide are really stable during dissolvation of the silica matrix. The latter could be the reason for the lower degree of ordering as compared with ordered mesoporous carbons, which prevents the formation of a long range ordered mesopore system that could be detected in small-angle X-ray diffractograms. Thus, further improvement of the infiltration process and removal of the silica matrix is needed. Especially a higher degree of filling and a selective deposition inside the pores is required for the preparation of well ordered inverse replicas. The latter could be achievable using catalytic CVI with the aid of transition metal particles inside the pores that accelerate the deposition inside the pores and is currently under investigation.

Conclusion

Summarizing, we have demonstrated the effective design of SiC/MCM-48 and SiC/SBA-15 nanocomposites using chemical vapor infiltration methods. The CVI process can be used to coat the mesoporous matrix with a nanosized coating on the inner or outer surface area by adjusting the deposition temperature. At lower temperature, SiC infiltration takes place predominately inside the pore system, but the crystallite size is too small to be detectable by means of wide-angle X-ray diffraction. At higher temperature, deposition is predominately observed on the outer surface of the particles leading to hedgehog-like core−shell particles with a hard protective coating of SiC on the outer surface and a soft inner core consisting of an ordered mesoporous MCM-48 matrix. For the hexagonal pore system, SBA-15, subsequent reduction of the specific pore volume and pore size with increasing duration of the deposition process indicates preferential deposition inside the pores in the form of an ultrathin pore coating. The infiltration process significantly increases the thermal stability of the host system, probably due to micropore filling in the early stages of the infiltration. Long-term infiltration results in a maximum weight gain of 111% and a reduction of the specific mesopore volume from 0.463 to 0.028 cm^3g^{-1}. However, a more in-depth analysis of the sorption data indicate inhomogeneous coatings for prolonged infiltration periods and high precursor evaporation rates as well as pore blocking mechanisms. The latter results in the formation of larger β-SiC crystallites on the outer surface of the porous particles. They are discerned in transmission electron micrographs and wide angle XRD powder patterns. XPS analyses of gradually infiltrated matrixes reveal the compositional complexity of the deposited material. In the early stages of the infiltration, silicon oxycarbide is formed. The thin oxycarbide coating provides an interface for further deposition of pure SiC. Dissolution of the silica matrix produces mesoporous SiC with high specific surface area and very high specific mesopore volume but the pores are not ordered on a long-range scale. A limited degree of ordering is detected in transmission electron micrographs, but further improvement of the infiltration is necessary for the manufacture of well ordered mesoporous SiC materials.

Acknowledgment. We thank F. Schüth for helpful discussions and financial support. We also thank Prof. R. Riedel and C. Fasel for carbon analyses of SiC samples.

CM034737+